ACS APPLIED MATERIALS & INTERFACES

Research Article

www.acsami.org

Surface Modification of PMMA to Improve Adhesion to Corneal Substitutes in a Synthetic Core−Skirt Keratoprosthesis

Andri K. Riau,[†,‡] Debasish Mondal,[‡] Gary H. F. Yam,[‡] Melina Setiawan,[‡] Bo Liedberg,[†,§] Subbu S. Venkatraman,[*,†] and Jodhbir S. Mehta[*,†,‡,∥,⊥]

[†]School of Materials Science and Engineering, Nanyang Technological University, Singapore 639798, Singapore

[‡]Tissue Engineering and Stem Cell Group, Singapore Eye Research Institute, Singapore 169856, Singapore

[§]Center for Biomimetic Sensor Science, Nanyang Technological University, Singapore 637553, Singapore

[∥]Singapore National Eye Center, Singapore 168751, Singapore

[⊥]Department of Clinical Sciences, Duke-NUS Graduate Medical School, Singapore 169857, Singapore

Supporting Information

ABSTRACT: Patients with advanced corneal disease do poorly with conventional corneal transplantation and require a keratoprosthesis (KPro) for visual rehabilitation. The most widely used KPro is constructed using poly(methyl methacrylate) (PMMA) in the central optical core and a donor cornea as skirt material. In many cases, poor adherence between the PMMA and the soft corneal tissue is responsible for device "extrusion" and bacterial infiltration. The interfacial adhesion between the tissue and the PMMA was therefore critical to successful implantation and device longevity. In our approach, we modified the PMMA surface using oxygen plasma (plasma group); plasma followed by calcium phosphate (CaP) coating (p-CaP); dopamine followed by CaP coating (d-CaP); or plasma followed by coating with (3-aminopropyl)triethoxysilane (3-APTES). To create a synthetic KPro model, we constructed and attached 500 μm thick collagen type I hydrogel on the modified PMMA surfaces. Surface modifications produced significantly improved interfacial adhesion strength compared to untreated PMMA ($p < 0.001$). The p-CaP group yielded the best interfacial adhesion with the hydrogel (177 ± 27 mN/cm^2) followed by d-CaP (168 ± 31 mN/cm^2), 3-APTES (145 ± 12 mN/cm^2), and plasma (119 ± 10 mN/cm^2). Longer-term stability of the adhesion was achieved by d-CaP, which, after 14 and 28 days of incubation in phosphate buffered saline, yielded 164 ± 25 mN/cm^2 ($p = 0.906$ compared to adhesion at day 1) and 131 ± 20 mN/cm^2 ($p = 0.053$), respectively. In contrast, significant reduction of adhesion strength was observed in p-CaP group over time ($p < 0.001$). All surface coatings were biocompatible to human corneal stromal fibroblasts, except for the 3-APTES group, which showed no live cells at 72 h of culture. In contrast, cells on d-CaP surface showed good anchorage, evidenced by the expression of focal adhesion complex (paxillin and vinculin), and prominent filopodia protrusions. In conclusion, d-CaP can not only enhance and provide stability to the adhesion of collagen hydrogel on the PMMA surface but also promote biointegration.

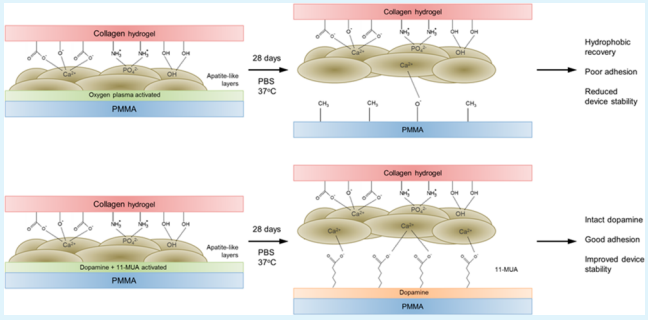

KEYWORDS: *collagen hydrogel, keratoprosthesis, adhesion, polymer, biointegration, dopamine, plasma treatment, hydrophobic*

INTRODUCTION

Corneal disease is a leading cause of blindness worldwide, second only to cataract.[1] Globally, it is estimated to be responsible for blindness in 4.9 million individuals, which is equivalent to 12% of the total 39 million who are blind.[1,2] Currently, the only effective treatment for the advanced corneal diseases is allogeneic corneal transplantation. However, donor corneal transplantation is often plagued with clinical, ethical and logistical limitations, such as the global shortage of transplantation-grade corneas,[3] or the necessary infrastructure for a transplantation service not being available in most countries due to a lack of storage facilities, or cultural and religious issues.[4,5]

The current surgical alternative to donor corneal transplantation is implantation of corneal prosthesis or keratoprosthesis (KPro). Several commercially available KPros have been used clinically with varying surgical complexity and success rate; however, the Boston KPro is the most widely used.[3,6] The design and material of conventional KPros vary, but most share a common feature in that poly(methyl methacrylate) (PMMA) is used as the primary material of the optical axis.[3,6] In these KPro constructs, the PMMA serves as the optical core to the surrounding donor corneal tissue (Figure 1A). The core−skirt

Received: April 11, 2015
Accepted: September 21, 2015
Published: September 21, 2015

DOI: 10.1021/acsami.5b07621
ACS Appl. Mater. Interfaces 2015, 7, 21690−21702

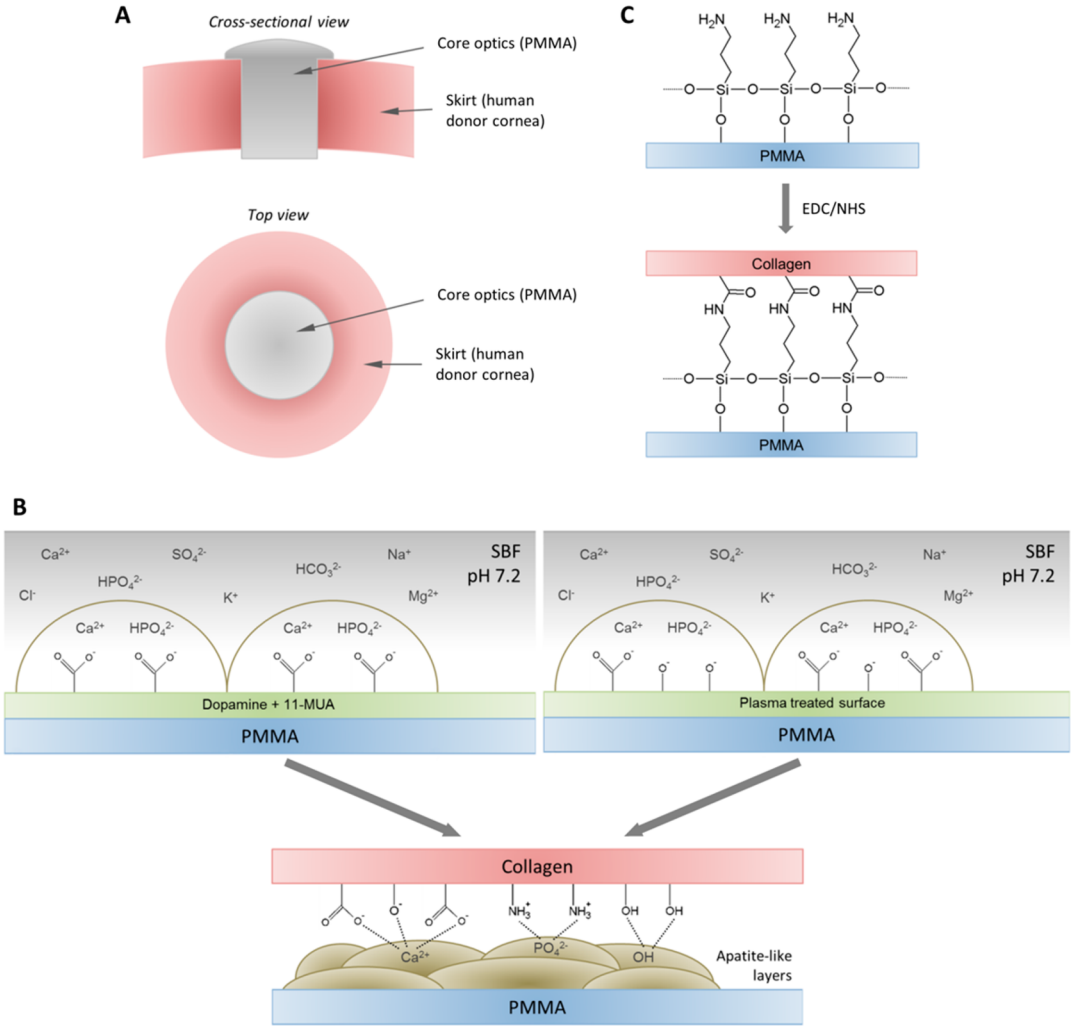

Figure 1. Illustrations of core−skirt keratoprosthesis (KPro) and mechanism of PMMA surface modification. (A) A core−skirt KPro consists of a core optical cylinder, made of PMMA, surrounded by skirt material, which conventionally is a human donor cornea. In our proposed synthetic KPro model, we utilized collagen type I hydrogel as donor corneal substitute. (B) Mechanism of apatite-like deposition on either dopamine+11-MUA functionalized surface (left panel) or oxygen plasma activated surface of PMMA (right panel) and subsequent interactions with the collagen hydrogel. (C) Mechanism of 3-APTES coating on oxygen plasma activated PMMA surface and its subsequent interactions with the collagen hydrogel.

constructional design has been shown to be one of the most successful designs, whereby the PMMA provides resistance to biodegradability of the device, and the surrounding corneal tissue allows for host tissue integration.[7] However, due to the surface properties of PMMA that are unfavorable for tissue adhesion, it has been a challenge to improve the skirt-PMMA integration. The combination of perpetual eyeball movement and blinking, and poor adhesion between PMMA and the surrounding tissue inevitably detaches the corneal tissue from the PMMA surface, allowing the possibility of epithelial downgrowth, bacterial infection, leakage of aqueous humor, and possibly leading to device failure.[8,9] Surface modifications of the PMMA surface can be used to create a surface that is compatible and more ready to interact with the corneal tissue. This will create a good adhesion between the two dissimilar materials and ultimately, reducing the long-term complications associated with KPro. Wang and colleagues attempted to address this shortcoming by coating the PMMA surface with hydroxyapatite (HAp), which was achieved by incubating the polymer in simulated body fluid (SBF).[10] Using in vitro mechanical testing, they showed that the force required to detach the corneal tissue from the HAp-coated PMMA cylinder was increased by almost 1.5 order of magnitude compared to noncoated PMMA.[10]

An alkoxysilane commonly used in the literature to attach proteins or soft materials on various types of hard material is (3-aminopropyl)triethoxysilane (3-APTES),[11,12] which ends in a primary amine group. The amine group can subsequently be modified with another cross-linker, such as glutaraldehyde, to produce a reactive group that binds to materials with amine ends, such as collagen. The amine group can also react with carbodiimide-activated carboxyl end of collagen to form a covalent linkage. DiVito and colleagues had developed a composite hydrogel made of a mixture of 3-APTES and collagen type I, which showed the ability to promote corneal epithelialization in rabbit corneas ex vivo.[13] Therefore, 3-APTES can be a candidate molecule to modify the PMMA surface to improve its adhesion with corneal tissue, which is predominantly constructed by collagen type I.[14]

In the current study, we used collagen type I hydrogel, instead of human corneal tissue, to study its adhesion on various modified PMMA surfaces as a KPro model. By using

DOI: 10.1021/acsami.5b07621
ACS Appl. Mater. Interfaces 2015, 7, 21690−21702

collagen hydrogel as donor corneal substitute, we could reduce our current heavy reliance on the donor corneas and also minimize long-term complications normally associated with the use of donor corneas. We attempted to show the potential improvements of interfacial adhesion between a surface modified rigid material and a soft material, and also to highlight a possibility to develop a synthetic KPro with PMMA core and collagen hydrogel skirt in the near future. The PMMA surface was modified using four different methods: (1) oxygen plasma irradiation; (2) surface activation with oxygen plasma, followed by calcium phosphate (CaP) deposition; (3) surface functionalization with dopamine and 11-mercaptoundecanoic acid (11-MUA), followed by CaP coating as described previously;[10] (4) surface activation with oxygen plasma, followed by 3-APTES coating. To assess the outcomes of the different coatings, we investigated the resulting interfacial adhesion strength, cytotoxicity of the surface coatings, and the biointegration of primary human corneal stromal fibroblasts on the modified PMMA.

EXPERIMENTAL SECTION

Oxygen Plasma Treatment of PMMA Surface. PMMA sheets with 0.5 mm thickness were purchased from Goodfellow (Huntingdon, England). The sheets were cut into 2 × 3 cm, washed in 70% ethanol for 15 min and extensively rinsed with distilled water. Oxygen plasma treatment was performed in a Covance multipurpose plasma system (Femto Science, South Korea). The samples were treated with radio frequency oxygen plasma with 200W power for 5 min. The PMMA sheets were placed between two parallel plate electrodes enclosed in a rectangular plasma reactor chamber. Air was removed with vacuum application for at least 30 min before the power was turned on. The pressure at the moment of plasma discharge was 0.2 Torr. The flow rate of oxygen was set at 20 standard cubic centimeters per minute (sccm). After the discharge stopped, oxygen gas flow was continued for a further 15 min to stabilize the resulting radicals and functional groups. This treatment method was referred to as the plasma group.

Coating of PMMA Surface with Calcium Phosphate. Two different methods were used to deposit CaP on the PMMA surface. In the first method, previously reported by Wang and colleagues,[10] the sterilized PMMA sheet (2 × 3 cm in size) was treated in 2 mg/mL dopamine (DOPA; Sigma-Aldrich, St. Louis, MO) in 10 mM Tris buffer, pH 8.5 (Sigma-Aldrich) overnight at room temperature followed by immersion in 50 μM of 11-mercaptoundecanoic acid (11-MUA; Sigma-Aldrich) for 4 h at room temperature before being placed in 1.5× simulated body fluid (SBF) solution at 37 °C for 14 days. The SBF was prepared according to the protocol described by Kokubo et al.[15] In brief, the SBF solution contains 213.0 mol/m^3 Na^+, 7.5 mol/m^3 K^+, 2.3 mol/m^3 Mg^{2+}, 3.8 mol/m^3 Ca^{2+}, 221.7 mol/m^3 Cl^-, 6.3 mol/m^3 HCO_3^-, 1.5 mol/m^3 HPO_4^{3-}, and 0.8 mol/m^3 SO_4^{2-}. The SBF solution was refreshed daily. After 14 days, the sheets were washed several times in distilled water, and dried in a vacuum incubator at 37 °C. This treatment was referred to as the d-CaP group.

In the second method, referred as the p-CaP group, instead of coating with dopamine and 11-MUA, the PMMA surface was treated with oxygen plasma for 5 min. The power setting and oxygen flow were as described in the preceding section. Following plasma treatment, the sheet was incubated in 1.5× SBF at 37 °C for 14 days and refreshed daily.

Coating of PMMA Surface with Alkoxysilane. Sterilized PMMA sheet (2 × 3 cm in size) was first treated with 5 min oxygen plasma (power setting and oxygen flow were as described in the earlier section). The PMMA sheet was immersed in 5% (v/v) 3-APTES (Sigma-Aldrich) in 70% ethanol overnight at room temperature. The sheet was then washed with 70% ethanol for 15 min, rinsed extensively with distilled water, dried in vacuum incubator at 37 °C, and finally placed in 90 °C incubator overnight to stabilize the coating layer. This treatment was referred to as the 3-APTES group.

Water Contact Angle Measurement. The water contact angle was measured by a contact angle goniometer (Analytical Technologies, Singapore) using a static sessile drop technique. At room temperature, distilled water was pumped out of a syringe at a rate of 5 μL/s and allowed to settle for 15 s on the samples before the image was taken. The contact angle was generated from the image with FTA32 software version 2.0 (build 276.2; Portsmouth, VA).

Analysis of Surface Morphology and Elemental Composition. The surface morphology of surface modified PMMA sheets was observed with a Nanoscope IIIa atomic force microscope (AFM; Digital Instruments, Santa Barbara, CA). Topographic images were captured in tapping mode employing monolithic silicon NCH-50 Point Probe (NanoWorld AG, Neuchatel, Switzerland). The scan size was set at 15 × 15 μm. The surface was scanned at a rate of 1 Hz with a resolution of 256 × 256 pixels. Three-dimensional topographic images and roughness (RMS value) data were obtained using Nanoscope image processing software version 5.12r5 (Digital Instruments).

For scanning electron microscopy (SEM), the PMMA sheets were mounted on a stub secured by carbon adhesive tape. The sheets were sputter-coated with a 10 nm thick layer of gold and examined with a JSM-6300F microscope (JEOL, Tokyo, Japan) at an accelerating voltage of 10 kV. Surface elemental composition was assessed by energy dispersive X-ray spectroscopy (EDX) attached to the microscope.

Attenuated Total Reflection-Fourier Transform Infrared Spectroscopy. Infrared (IR) spectra of the modified PMMA surfaces were collected in the range from 4000 to 650 cm^{-1} using a PerkinElmer Frontier FTIR spectrometer (Waltham, MA). The spectrometer was equipped with an ATR sampling universal accessory supplied with a top plate for ZnSe crystal. The plate was cleaned with 70% ethanol after each spectrum was acquired. The PMMA sheet was placed on the plate and tightened down to the 40% gauge mark shown on the software for the instrument. Spectra were obtained with 16 scans and 4 cm^{-1} resolution.

Casting of Collagen Hydrogel on Modified PMMA Surface. Casting of collagen hydrogel on the modified PMMA surfaces was performed immediately after surface modification. The collagen hydrogel was constructed as described previously.[16] Bovine atelocollagen type I was purchased from Koken (Tokyo, Japan). Briefly, 0.5 mL aliquot of 10% (w/v) atelocollagen in acidic solution (pH 3.0) was loaded into a syringe mixing system. The collagen solution was adjusted to pH 5.0 with 1N NaOH, followed by thorough mixing by pumping the syringes. Calculated amounts of 10% (w/v) 1-ethyl-3-(3-(dimethylamino)propyl) carbodiimide (EDC; Sigma-Aldrich, St. Louis, MO) and 10% (w/v) *N*-hydroxysuccinimide (NHS; Sigma-Aldrich) were added to produce a 2:1 molar ratio of EDC to NHS and mixed with the collagen solution. The mixed solution (0.1 mL) was dispensed onto the center of the PMMA sheet and flattened with a glass slide, resulting in a cylindrically shaped hydrogel. The thickness of the hydrogels was consistently maintained by placing 0.5 mm thick spacers under the glass side at the edges of the modified PMMA sheet. The hydrogel was cured in a humidified chamber at room temperature for 24 h before being subjected to the shear bond strength test. Two groups that yielded the best adhesion to the PMMA and untreated PMMA were subjected for a longer term study, whereby the hydrogel-modified PMMA constructs were incubated in 0.01 M phosphate buffered saline (PBS) at 37 °C for 14 and 28 days, with PBS refreshed daily.

Shear Bond Strength Test. Samples (hydrogel adhered on PMMA sheets; n = 5 of each group) were secured at the base of a Chatillon tensile tester (Largo, FL). The position of the sample was adjusted until the chisel-shaped fixture, attached to the 10 N load cell, aligned at the center of the hydrogel at the bonding interface. The crosshead speed was set at 5 mm/min. The test was stopped, and the maximum force was recorded when the hydrogel was completely detached from the surface of PMMA sheets.

DOI: 10.1021/acsami.5b07621
ACS Appl. Mater. Interfaces 2015, 7, 21690−21702

Culture and Seeding of Corneal Stromal Fibroblasts. Research grade cadaveric corneal tissues were purchased from Lions Eye Institute for Transplant and Research (Tampa, FL). They were preserved in Optisol-GS (Bausch & Lomb Surgical, Irvine, CA) and transported at 4 °C to the laboratory. Central button (8 mm in diameter) was trephined and treated with Dispase II (20 mg/mL, Roche, Basel, Switzerland) followed by gentle scraping to completely remove corneal epithelium and endothelium. The stromal tissue was trimmed into small pieces and digested with collagenase I (1 mg/mL, Worthington, Lakewood, NJ) in DMEM/F12 (Life Technologies, Carlsbad, CA) for 9−12 h at 37 °C. Single cells were cultured in DMEM/F12 containing 10% fetal bovine serum (FBS; Life Technologies) and 1% antibiotic/antimycotic (penicillin, streptomycin sulfate, and amphotericin B; Life Technologies). At passages 3−5, the stromal fibroblasts (1000 cells/cm^2) was seeded on sterile modified PMMA sheets and cultured for 24 h and 72 h before further tests. Cells seeded on sterile glass coverslips were considered as control.

Cell Proliferation Assay. Proliferation of corneal fibroblasts on modified PMMA surfaces was assessed using a 5-ethynyl-2′-deoxyuridine (EdU) assay kit (Life Technologies) according to the manufacturer's protocol. In brief, the cells were incubated in EdU (10 μM) containing medium for 24 h. They were then washed with PBS, fixed with 4% paraformaldehyde (Sigma), followed by blocking and permeabilization in 0.1% Triton X-100 (Sigma) in 3% bovine serum albumin (Sigma) at room temperature. Incorporated EdU was detected by Alexa Fluor 488 fluorescent-azide coupling Click-iT reaction.[17] Finally, the samples were mounted in Fluoroshield containing DAPI (4′,6-diamidino-2-phylindole; Santa Cruz Biotechnology, Santa Cruz, CA) and viewed under Zeiss AxioImager Z1 fluorescence microscope (Carl Zeiss, Oberkochen, Germany) at 200× magnification. The total number of cells and EdU-positive cells were quantified from three random fields of each sample (n = 3 of each group).

Cell Viability on Modified PMMA Surface. The cytotoxicity was analyzed using Live/Dead Viability/Cytotoxicity assay kit (Life Technologies) according to the manufacturer's protocol. In brief, the cells were incubated with calcein AM and ethidium homodimer-1 (EthD-1) for 45 min, washed, and mounted in Fluoroshield containing DAPI. Samples were viewed using a Zeiss AxioImager Z1 fluorescence microscope (Carl Zeiss) at 100× magnification. Live cells were stained green by calcein AM, and dead cells were stained red by EthD-1. Both live and dead cells were quantified from 2 random fields on each sample (n = 3 of each group), and the live/dead cell ratio was calculated. In addition, initial cell attachment efficiency was calculated by using the following formula:

$$\text{cell attachment efficiency (\%)} = \left(\frac{n_{\text{actual}}}{n_{\text{theoretical}}}\right)100$$

where n_{actual} is the actual number of cells in the viewing field, and $n_{\text{theoretical}}$ is the theoretical number of cells expected to attach in the viewing field, which, in a 100× viewing field (4.5 × 3.5 mm) was equivalent to 157 after accounting for the 1000 cells/cm^2 seeding density.

Immunocytochemistry of Cell Attachment Markers. Cells on glass coverslips and surface modified PMMA sheets were fixed with freshly prepared neutral buffered 2% paraformaldehyde (Sigma-Aldrich). After quenching of free aldehyde with 50 mM ice-cold ammonium chloride and PBS washes, cells were permeabilized and blocked with PBS containing 0.425% saponin (Sigma-Aldrich), 1% bovine serum albumin (BSA; Sigma-Aldrich) and 2% normal goat serum (Life Technologies), followed by incubation of primary antibodies: mouse monoclonal antipaxillin (Millipore, Billerica, MA) and mouse monoclonal antivinculin (Sigma-Aldrich). After PBS washes, cells were incubated with donkey antimouse IgG AlexaFluor 488-conjugated secondary antibody (Jackson ImmunoRes Lab, West Grove, PA) and AlexaFluor 568-conjugated phalloidin (Life Technologies). The samples were mounted in Fluoroshield containing DAPI and viewed under Zeiss AxioImager Z1 fluorescence microscope (Carl Zeiss).

Statistical Analysis. Data were expressed as mean ± standard deviation (SD). Statistical significance between groups was calculated by one-way ANOVA and post hoc Tukey comparison test. A value of $p < 0.05$ was considered to be statistically significant. All statistical analysis was performed using SPSS software (version 17.0, SPSS Inc., Chicago, IL).

RESULTS AND DISCUSSION

General Consideration for Choosing Surface Modification Methods. PMMA is one of the more commonly used materials in biomedical applications, for instance in craniofacial reconstruction,[18] as corneal prosthetic device,[19] and as bone cement.[20] However, tissue and cell biointegration with PMMA is generally poor due to the relatively hydrophobic surface property of the polymer and the lack of active functional groups.[21,22] In fact, the poor tissue−PMMA interaction has been shown to be responsible for the failure of a KPro device in the ophthalmic application.[8,9] Surface modification can be an effective method to improve the biointegration capacity of PMMA without excessively altering the bulk properties of the polymer.[21,22] Dopamine, a versatile underwater adhesive, can form on a variety of surfaces and further induce CaP deposition in SBF.[23] The addition of 11-MUA with carboxyl ends creates a negatively charged surface, which can enhance the dopamine-coated PMMA surface as nucleation site for CaP deposition (Figure 1B, left panel). Similar to functionalization with dopamine and 11-MUA, the activation of PMMA with oxygen plasma produces negatively charged surface via the creation of surface carboxyls and hydroxyls, which in turn acts as nucleation site for CaP (Figure 1B, right panel). Electrostatic bonding is proposed to be the main driving force for the interaction of CaP to collagen, while adsorption of functional binding groups of collagen by CaP and hydrogen bonding can be formed as secondary interaction forces (Figure 1B).[24,25] In addition, the surface roughness of CaP-coated PMMA also cannot be ruled out in improving its interfacial adhesion to collagen.

Surface hydroxyls resulted from oxygen plasma treatment can also undergo condensation reaction with silanols of the 3-APTES (Figure 1C). The amine ends of 3-APTES coating can subsequently be covalently bonded to the carboxyls, which are abundantly present in the collagen, via carbodiimide chemistry (Figure 1C).

We had initially attempted to construct the collagen hydrogel, followed by bringing the hydrogel in contact with the modified PMMA in order to mimic the construction of the conventional KPro. However, the hydrogel could not form any adhesion with the underlying PMMA, regardless of the surface coatings. Adhesion could only be achieved when the hydrogel was allowed to cross-link and settle overnight on the PMMA surface.

Oxygen Plasma Treatment to Activate PMMA Surface. We first investigated the effect of oxygen plasma treatment on the surface hydrophilicity of PMMA and determined the optimized plasma treatment time to activate the PMMA surface prior to further surface modifications. The surface hydrophilicity level of PMMA increased after a 2 min plasma treatment, which yielded water contact angle of 43.4 ± 5.8° and the contact angle reduced further after a 5 min treatment to 24.6 ± 1.1° (both $p < 0.001$ relative to untreated PMMA) (Figure S1A). Increasing the treatment time beyond 5 min produced a diminishing return in terms of hydrophilicity level, evident by higher water contact angle after 10 min treatment

DOI: 10.1021/acsami.5b07621
ACS Appl. Mater. Interfaces 2015, 7, 21690−21702

(42.0 ± 1.5°) compared to that after 5 min treatment (Figure S1A). This return was attributed to a substantial change in surface morphology (see AFM analysis below) rather than to a reduction in the amount of O−H functional groups that formed by increasing plasma treatment time beyond 5 min (see surface IR analysis below). On AFM, it was revealed that surface roughness increased with plasma treatment time, where the 2 min plasma treatment produced a roughness of 9.7 ± 1.0 nm (p < 0.001 relative to untreated PMMA) (Figure S1B), the 5 min plasma treatment produced a roughness of 18.7 ± 1.0 nm (p < 0.001 relative to untreated PMMA) (Figure S1B), and the 10 min plasma treatment increased the roughness to 31.7 ± 2.5 nm (p < 0.001 relative to untreated PMMA) (Figure S1B). This finding is consistent with a previously published study.[26] Figure S1C summarizes the average roughness of untreated PMMA and plasma-treated PMMA surfaces by AFM in a bar graph. Moreover, the 10 min plasma-treated PMMA appeared opaque due to prolonged surface plasma etching, rendering it not suitable for corneal prosthetic use (Figure S1D).

We then investigated the surface IR spectra of the untreated PMMA and the PMMA treated with plasma for different periods of time. Small differences in the resulting surface IR spectra could be seen in certain spectral regions (Figure S2). First, there was a clear difference in the relative intensity of the peak between 3650 and 3350 cm^{-1}, attributable to O−H functional group (Figure S2A). To further delineate the differences, we performed spectral subtraction of the untreated PMMA from the plasma-treated PMMA in the 2400−4000 cm^{-1} region. The subtraction factor was adjusted for each subtraction until the strong CH_3 peaks in the region of 2800−3100 cm^{-1} were canceled out. The subtraction process revealed that plasma treatment for 2, 5, and 10 min produced a broad band peaking near 3400 cm^{-1}, and highest intensities were seen after 5 and 10 min plasma treatment (Figure S2B). This broad peak is characteristic of H_2O, suggesting that the amount of water attached to the plasma-treated PMMA increased with treatment time. A second spectral intensity difference was seen between 2951 and 2995 cm^{-1} (C−H stretching modes), where the untreated PMMA produced the highest peak intensity, followed by plasma 2 min, plasma 5 min and plasma 10 min (Figure S2C), suggesting that $-CH_3$ terminal functional groups were more abundant on untreated surface compared to the plasma treated PMMA. The reduction of peak intensities was in line with the formation of O−H groups due to partial oxidation of the PMMA surface. The FTIR results were corroborated by EDX analysis, showing a reduction of percentage of C atom and an elevation of percentage O atom with increasing plasma treatment time (Table S1). To provide PMMA surface with sufficient hydrophilicity and to avoid opaqueness due to increasing surface roughness, we selected and performed oxygen plasma treatment for 5 min to activate the PMMA surface before further surface modifications.

Surface Hydrophilicity Following Surface Modification. The surface hydrophilicity of PMMA after various surface modifications is summarized in Table 1. The treatment that yielded the highest surface hydrophilicity (as measured by reduced water contact angle relative to untreated PMMA) was p-CaP group (2.7 ± 3.1°) and d-CaP group (2.7 ± 3.1°), followed by plasma group (24.6 ± 1.1°) (Figure 2). One-way ANOVA with posthoc Tukey test revealed that all surface modification techniques significantly reduced the water contact angle compared to untreated PMMA (p < 0.001), except the 3-APTES group. Treatment with 3-APTES did not change the water contact angle (72.0 ± 0.9°) significantly in comparison to untreated PMMA (68.4 ± 3.0°; p = 0.286), which was consistent with a previous study.[27]

Table 1. Surface Wettability of Untreated PMMA and Modified PMMA

	water contact angle (deg)	p value[a]
untreated PMMA	68.4 ± 3.0	
plasma	24.6 ± 1.1	2.07×10^{-12}
d-CaP	2.7 ± 3.1	1.28×10^{-12}
p-CaP	2.7 ± 3.1	1.28×10^{-12}
3-APTES	72.0 ± 0.9	0.286

[a]Significant difference relative to untreated PMMA. p < 0.05 was considered to be statistically significant.

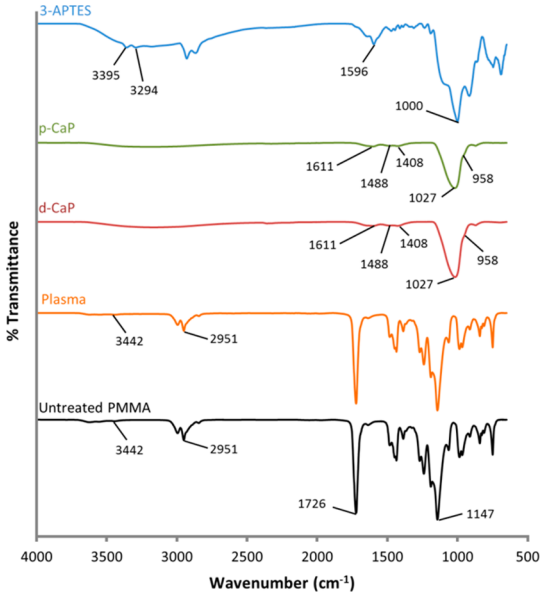

Figure 2. Infrared (IR) spectra of surface modified PMMA. Comparison of surface IR spectrum obtained from (black) untreated PMMA and modified PMMA by (orange) oxygen plasma, (red) dopamine + calcium phosphate (CaP) coating, (green) oxygen plasma + CaP coating, and (blue) 3-APTES.

Surface Infrared Spectra and Elemental Composition after Surface Modification. The surface IR spectra of untreated PMMA and differentially modified PMMA surfaces are shown in Figure 2. Untreated PMMA showed distinct spectral peaks near 1100−1300 and 1726 cm^{-1}, which were attributed to the presence of C−O and C=O stretching modes of the ester group, respectively. In addition, a spectral peak at 2951 cm^{-1} indicated the C−H stretching of PMMA. Spectral peaks of PMMA were not that prominent in the p-CaP and d-CaP groups due to the relatively thick coating layer, which almost completely masked the PMMA surface. A peak at 1027 cm^{-1} and a weak shoulder at 958 cm^{-1} in both groups were attributed to the P−O group of CaP. The peak at 1027 cm^{-1} in d-CaP group appeared to have slightly higher intensity than that in p-CaP group. Three peaks at 1611, 1488, and 1408 cm^{-1}, corresponding to the carbonate group of the CaP coating, could also be observed. In the 3-APTES group, spectral peaks appeared at 3294 and 3395 cm^{-1}, indicating the presence of the primary amine group of 3-APTES. Moreover, a peak at 1596 cm^{-1} confirmed the presence of primary amine groups (N−H bending mode) attributed to 3-APTES coating. A sharp

DOI: 10.1021/acsami.5b07621
ACS Appl. Mater. Interfaces 2015, 7, 21690−21702

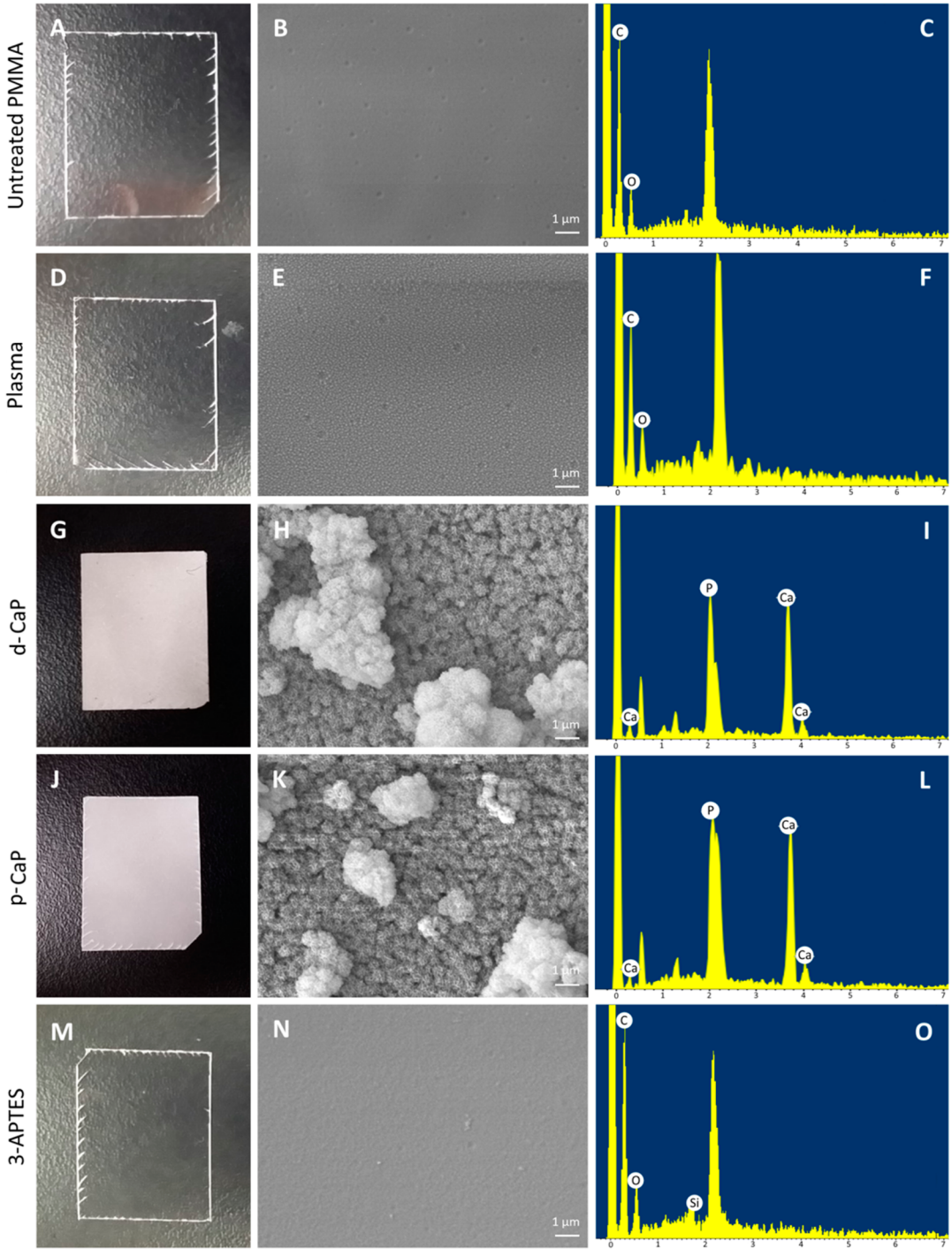

Figure 3. Morphology and elemental composition of surface-modified PMMA assessed by SEM and EDX. (A, D, G, J, and M) Macroscopic appearance of untreated and surface-modified PMMA sheets. (B, E, H, K, and N) SEM images of untreated and surface modified PMMA sheets. (C, F, I, L, and O) EDX spectrographs showing surface elemental composition of untreated and surface modified PMMA.

Table 2. Surface Composition of Untreated PMMA and Modified PMMA Detected by EDX

	C	O	Ca	P	Si
untreated PMMA	71.2 ± 0.3%	28.8 ± 0.3%			
plasma	69.7 ± 0.8%	30.3 ± 0.8%			
d-CaP			54.8 ± 0.6%	45.2 ± 0.6%	
p-CaP			56.4 ± 1.2%	43.6 ± 1.2%	
3-APTES	60.9 ± 2.0%	28.9 ± 1.3%			10.2 ± 1.0%

DOI: 10.1021/acsami.5b07621
ACS Appl. Mater. Interfaces 2015, 7, 21690−21702

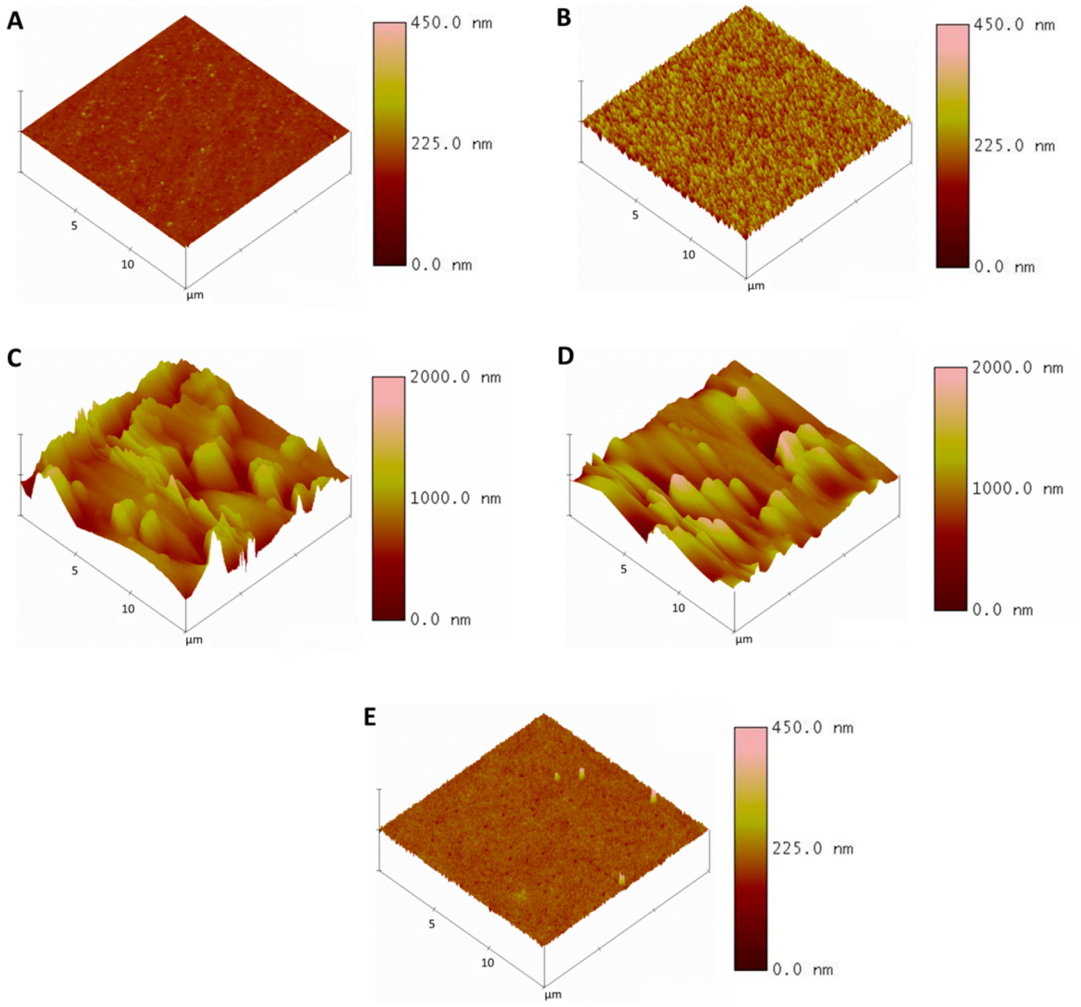

Figure 4. Surface roughness of untreated and modified PMMA analyzed with AFM. (A) Untreated PMMA. (B) Plasma group. (C) d-CaP group. (D) p-CaP group. (E) 3-APTES group.

peak at 1000 cm^{-1} indicated the presence of Si−O−Si on the aminosilane modified PMMA surface.

Consistent with the FTIR analysis, EDX spectroscopy demonstrated a reduction of C atoms and increased O atoms in the plasma group (Figure 3F) compared to untreated PMMA (Figure 3C), which suggested the creation of surface O−H groups by oxygen plasma treatment. EDX further corroborated our FTIR analysis, which showed relatively more phosphate groups produced by d-CaP than p-CaP. This resulted in lower Ca/P ratio in d-CaP group (1.21 ± 0.03) (Figure 3I) and p-CaP (1.29 ± 0.06) (Figure 3L). However, the difference in Ca/P ratio was not significantly different (p = 0.069). EDX revealed the presence of 10.2 ± 1.0% Si atoms in the 3-APTES group (Figure 3O). The atomic composition of untreated and modified PMMA surfaces is summarized in Table 2.

Surface Morphology and Roughness after Surface Modification. Macroscopically, plasma (Figure 3D) and 3-APTES (Figure 3M) treated PMMA appeared transparent and similar to untreated PMMA (Figure 3A). In contrast, d-CaP (Figure 3G) and p-CaP (Figure 3J) appeared opaque and were completely covered by the bone-like apatite. Under SEM, nanosized particles, indicative of bone-like apatite growth,[28] were seen covering the entire PMMA surface of d-CaP (Figure 3H) and p-CaP (Figure 3K). Agglomerates of the particles were present in some regions, attributing to the surface roughness of both CaP-coated surfaces. This observation was confirmed by cross-sectional SEM image of d-CaP (Figure S3A) and p-CaP (Figure S3B), which revealed that multilayered particles in some regions were thicker than those in other regions due to agglomeration of the apatite-like particles. AFM showed an average roughness of 343 ± 88 nm for d-CaP group (Figure 4C) and 301 ± 34 nm for p-CaP group (Figure 4D). No significant difference was found between d-CaP and p-CaP groups (p = 0.235).

The untreated PMMA surface appeared relatively smooth under both SEM (Figure 3B) and AFM (Figure 4A), interspersed with some nanosized grooves. Nanoscale surface undulations created by plasma etching were observed in the plasma group (Figure 3E). Under AFM, there was an increase in surface roughness after 5 min plasma treatment (18.7 ± 1.0 nm; Figure 4B). As shown in SEM images, coating with 3-APTES smoothed the initially plasma etched surface, evidenced by the barely visible nanoscale undulations seen in the plasma group earlier (Figure 3N). This was confirmed by AFM, which showed a significantly smoother surface in 3-APTES group (8.1 ± 1.1 nm; Figure 4E) compared to the plasma group (p < 0.001). The mean RMS values for untreated and all modified PMMA surfaces are summarized in Table 3.

DOI: 10.1021/acsami.5b07621
ACS Appl. Mater. Interfaces 2015, 7, 21690−21702

Table 3. Surface Roughness of Untreated PMMA and Modified PMMA

	mean RMS (nm)	p value[a]
untreated PMMA	1.5 ± 0.3	
plasma	18.7 ± 1.0	5.83×10^{-13}
d-CaP	342.8 ± 88.1	2.74×10^{-6}
p-CaP	300.7 ± 34.1	4.66×10^{-9}
3-APTES	8.1 ± 1.1	2.84×10^{-8}

[a]Significant difference relative to untreated PMMA. $p < 0.05$ was considered to be statistically significant.

Adhesion of Collagen Hydrogel on Modified PMMA Surface. The experimental setup used in our study to obtain the adhesion strength of collagen hydrogel, that was casted on untreated and modified PMMA surfaces, is depicted in Figure 5A. The maximum force required to detach the hydrogel completely from the PMMA surfaces was recorded and the adhesion strength in mN/cm^2 was calculated. Figure 5B summarizes the resulting interfacial bonding strength, measured 1 day after the hydrogels were casted on untreated and modified PMMA surfaces. There was significant improvement in the interfacial bonding strength after any surface modification ($p < 0.001$ compared to untreated PMMA). CaP coating of PMMA, either pretreated with plasma or dopamine and 11-MUA, produced the best bonding strength to collagen hydrogel (177 ± 27 mN/cm^2 for p-CaP group and 168 ± 31 mN/cm^2 for d-CaP group). No significant difference was found between p-CaP and d-CaP groups ($p = 0.647$). However, d-CaP ($p = 0.010$) and p-CaP ($p < 0.001$) produced significantly stronger interfacial adhesion than the plasma group. Coating with 3-APTES yielded the next best adhesion strength (145 ± 12 mN/cm^2), followed by plasma treatment (119 ± 10 mN/cm^2).

The KPro is designed to survive for a long period of time in patients. Therefore, it is paramount to assess the stability of the coating and the interfacial adhesion between the modified PMMA and hydrogel. We selected the two coating methods, that yielded the best adhesion strength from the tests performed 1 day after hydrogel casting, for a longer term study. Interestingly, we found that d-CaP produced a more stable adhesion with collagen over time (Figure 5B). At day 14, the adhesion was 164 ± 25 mN/cm^2 ($p = 0.906$ relative to adhesion at day 1) and was slightly reduced to 131 ± 20 mN/cm^2 at day 28 ($p = 0.053$). In contrast, the hydrogel adhesion strength on p-CaP was significantly reduced at day 14 (86 ± 26 mN/cm^2; $p < 0.001$ compared to day 1 adhesion) and was further reduced at day 28 to 66 ± 22 mN/cm^2. For both time points, the d-CaP produced significantly better adhesion than the p-CaP ($p = 0.001$). As expected, pristine PMMA could not provide long-term stability on the interfacial adhesion. Most of the hydrogels casted on untreated PMMA floated after a few days incubation in the PBS.

We conducted further study to seek for an explanation of the reduction of interfacial adhesion in the postincubation p-CaP group. Macroscopically, the CaP coating on the d-CaP group remained intact at day 28, except the region where the hydrogel lied on (Figure S4A). It appeared that the CaP coating was attached to and removed along with the hydrogel. A contrasting observation made on the p-CaP group revealed that most of the CaP coating was lifted off during the incubation process (Figure S4A). When we conducted water contact angle tests on the region where the hydrogel used to lie on, we found that d-CaP (day 14) and d-CaP (day 28) had similar wettability to the dopamine and 11-MUA activated PMMA (d-PMMA) (Figure S4B). However, the surface of the bare p-CaP (day 14) and p-CaP (day 28) had become more hydrophobic than the surface after plasma treatment (both $p < 0.001$; Figure S4B). FTIR

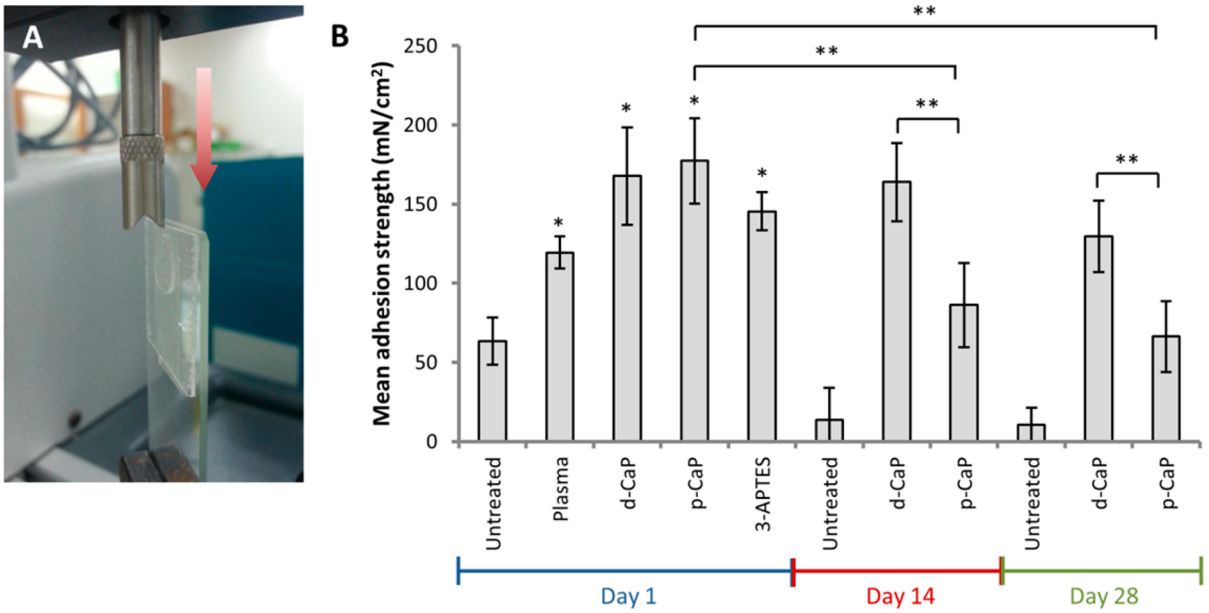

Figure 5. Shear adhesion strength of collagen hydrogel on surface modified PMMA. (A) Snapshot of the adhesion strength test setup. A chisel-shape fixture was attached to the load cell of a Chatillon tensile tester. The downward movement of the fixture would displace the hydrogel and eventually detach it from the PMMA surface. (B) Bar graph depicting the interfacial adhesion strength after various PMMA surface modifications. The d-CaP and p-CaP groups, which yielded the best adhesion strengths, were subjected for longer term study, whereby the hydrogel-modified PMMA constructs were incubated in PBS at 37 °C for a further 14 and 28 days. At the end of each time point, shear adhesion tests were then performed on the constructs. Height of error bars indicates standard deviation of means. *$p < 0.001$ in comparison to untreated PMMA group. **$p < 0.001$.

DOI: 10.1021/acsami.5b07621
ACS Appl. Mater. Interfaces 2015, 7, 21690−21702

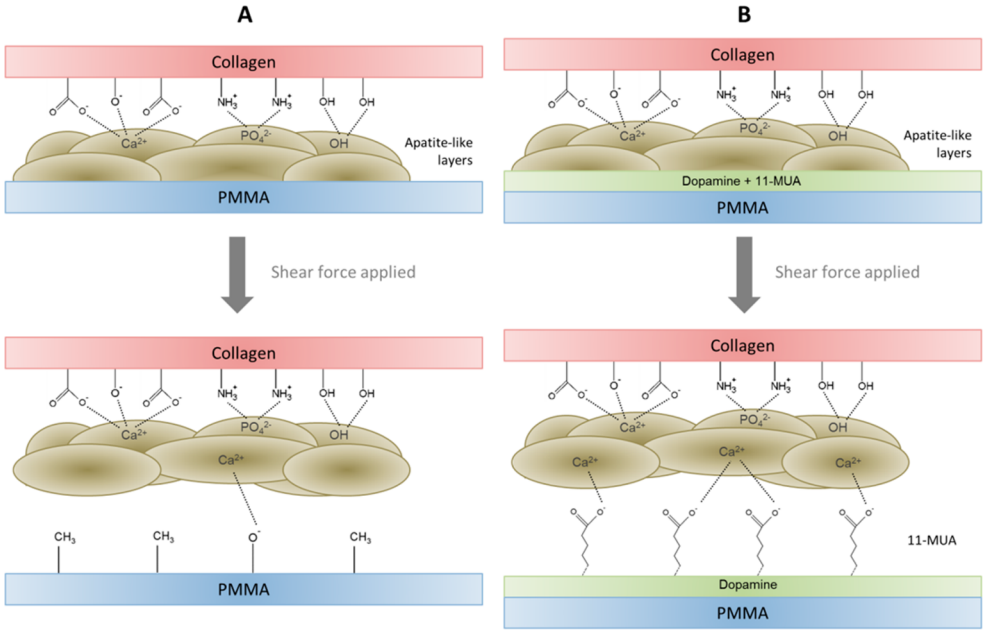

Figure 6. Illustrations showing mechanism of interactions between collagen and bone-like apatite deposited on two differentially activated PMMA surfaces after 28 days of incubation in PBS. (A) p-CaP group. (B) d-CaP group. Hydrophobic recovery and degradation of O−H functional groups on p-CaP weakened the anchorage of the CaP on the PMMA, reducing the hydrogel adhesion on p-CaP significantly compared to d-CaP.

performed on the bare d-CaP (day 14) and p-CaP (day 28) site showed characteristic peaks, albeit relatively weak bands, of phenyl group due to the presence of dopamine, such as the overtones from 1850 to 1750 cm^{-1} and the aromatic C−C stretch from 1600 to 1500 cm^{-1} (Figure S4C, right panel). The IR spectrum of d-CaP (day 14) and d-CaP (day 28) appeared similar to d-PMMA, where there was a lack of C−H stretching peaks (2951 and 2995 cm^{-1}) of the pristine PMMA (Figure S4C, left panel). Due to difficulty in assigning distinct spectral peaks in the p-CaP (day 14) and p-CaP (day 28) groups with FTIR, we performed EDX on the bare surface site to assess the difference in surface atomic composition of the postincubation p-CaP. There was a decrease in the percentage of oxygen composition on postincubation p-CaP compared to the plasma treated PMMA (Figure S4D). By taking the increased water contact angle and decreased number of O atoms on the postincubation p-CaP into consideration, we can postulate that there was a recovery of surface hydrophobicity after a period of time on the plasma activated surface, even with CaP deposited on it. This could be due to the degradation of the plasma-induced O−H group over time in PBS, a phenomenon well-documented in the literature.[29,30] Due to the hydrophobic surface and lack of active functional groups on which to anchor, the CaP coating could be easily peeled off and ultimately reduced the adhesion of hydrogel on the p-CaP (Figure 6A). On the other hand, although the CaP was lifted off along with the hydrogel, the dopamine and 11-MUA still remained grafted on the surface, providing better anchorage to the CaP coating (Figure 6B). Hence, the d-CaP resulted in better hydrogel adhesion over time compared to the p-CaP.

In our study, aminosilane produced the next best adhesion strength after d-CaP and p-CaP. The terminal $-NH_2$ functional groups of 3-APTES could form amide bonds with −COOH functional groups, which are present in collagen type I, via carbodiimide chemistry and as a result, enhanced the bonding strength between collagen hydrogel and PMMA. The amide bonds, which are generally stronger than hydrogen and electrostatic bonds, should have resulted in stronger adhesion strength than the CaP-coated PMMA. The reason for our contradictory finding may be 2-fold. First, the coating thickness of 3-APTES after overnight deposition is usually in the range of 10−15 nm.[31] The extremely thin coating was most likely not as effective in bearing the weight of the hydrogel vertically as the much thicker CaP coating, which can be in the range of 20−40 μm thick after 14 days of deposition in SBF (Figure S3). Second, most of the free carboxyl groups of the collagen were already cross-linked to the amine groups of the collagen when the solution was dispensed on the 3-APTES-modified PMMA surface,[32] leaving only a little carboxyl groups to react with terminal amine groups of the 3-APTES.

Cell Viability and Cell Proliferation on Modified PMMA Surface. As part of the optical core of a KPro, the modified PMMA surface will be transplanted in corneal stroma. Thus, it is necessary to study if the surface coating affects stromal properties, such as cytotoxicity and stromal cell proliferation. In Figure 7A, we show the in vitro effect of the PMMA surface modifications on the proliferation of human corneal stromal fibroblasts at 48 h and the cell viability at 24 and 72 h postseeding. The cells grown on glass coverslips, acting as the control group, showed a proliferative capacity of 62 ± 14% and negligible cell death at both 24 and 72 h time points. On untreated PMMA, relatively few cells were detected and the proliferation rate was reduced to 43 ± 10% ($p = 0.033$ relative to control). In addition, the live/dead cell ratio at 24 and 72 h postcell seeding was about 50%, and they were significantly less than the control group at the respective time point ($p < 0.001$). Cell proliferation and viability of plasma, d-CaP, and p-CaP groups were not significantly different than the control group. On 3-APTES coated surface, more live cells were found 24 h postseeding; however, fewer cells were seen at 48 h postseeding. The cell proliferation rate was significantly reduced (31 ± 15%; $p < 0.001$). After 72 h of culture, no live cells were detected, suggesting that 3-APTES coating might have a latent cytotoxic effect. This could be related to the

DOI: 10.1021/acsami.5b07621
ACS Appl. Mater. Interfaces 2015, 7, 21690−21702

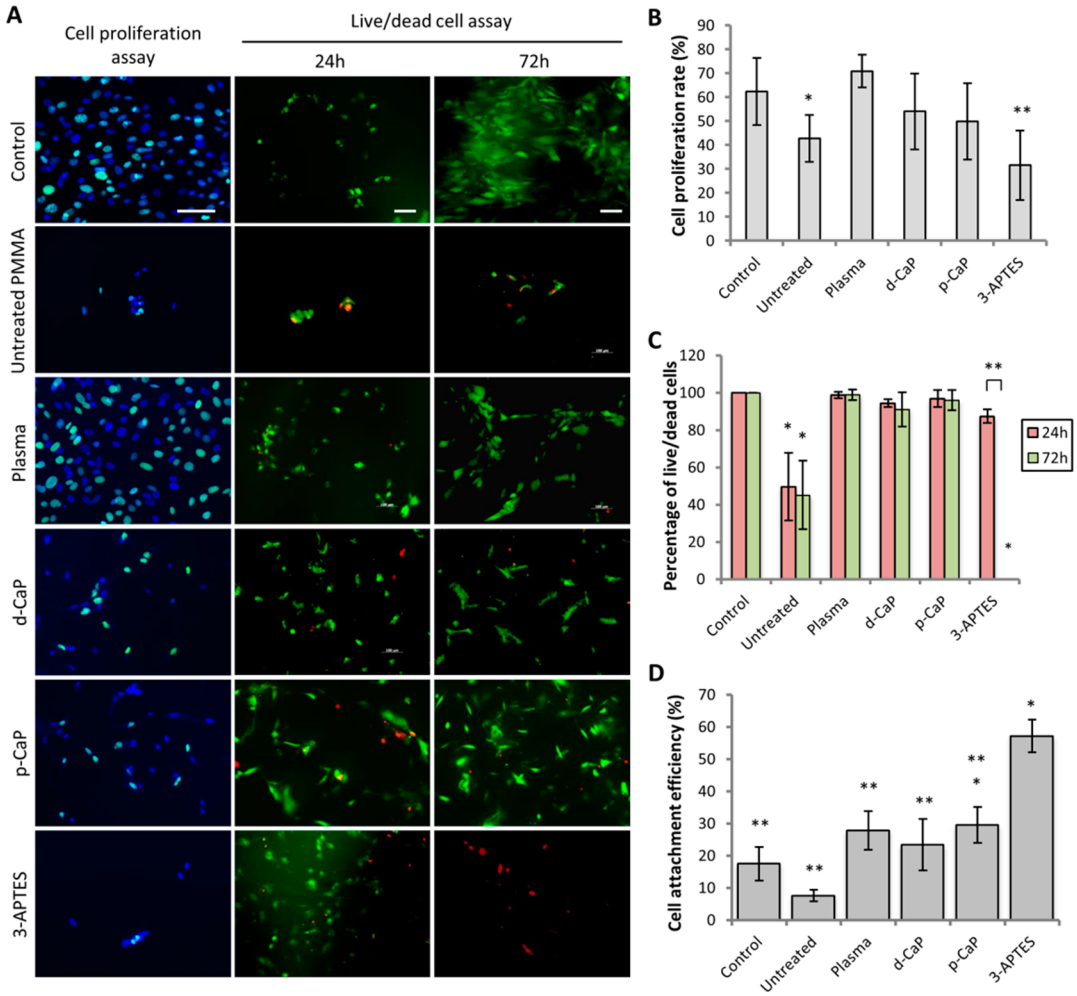

Figure 7. Viability and proliferation rate of human corneal fibroblasts on surface modified PMMA. (A, left) Proliferative corneal fibroblasts on 48 h after cell seeding on differentially modified PMMA surfaces. Green fluorescence indicates proliferating cells, whereas blue fluorescence shows cell nuclei. Live/dead cell assay performed on primary human corneal fibroblasts (center) 24 and (right) 72 h after cell seeding. Green fluorescence indicates live cells, whereas red fluorescence indicates dead cells. Scale bars = 100 μm. (B) Percentage of cell proliferation rate on untreated and modified PMMA surfaces. Height of error bars indicate standard deviation of means. *$p < 0.05$ in comparison to control. **$p < 0.001$ in comparison to control. (C) Quantification of live/dead cell ratio (red) 24 and (green) 72 hours after cell seeding. *$p < 0.001$ compared to control. **$p < 0.001$ compared to live/dead cell ratio after 24 h of culture on 3-APTES-treated PMMA. (D) Percentage of cell attachment efficiency on untreated and modified PMMA surfaces on 24 h after cell seeding. *$p < 0.001$ in comparison to control. **$p < 0.001$ in comparison to 3-APTES group.

partial hydrolysis and the presence of leachable toxic products of 3-APTES during cell culture.[33] The summary of cell proliferation rate and live/dead cell ratio for all treatment groups are depicted in Figure 7B,C.

From the live/dead cell assay, we also measured the initial cell attachment efficiency on the modified PMMA surfaces. Figure 7D showed an efficiency of 17.52 ± 5.21% for the control group. Untreated PMMA with hydrophobic surface had the significantly lowest cell attachment efficiency (7.62 ± 1.83%; $p < 001$) compared to any other group. The efficiency increased after PMMA surface modifications. However, only p-CaP (29.59 ± 5.58%) and 3-APTES (57.14 ± 5.06%) treatments significantly improved the efficiency compared to the control (both $p < 0.001$). The presence of $-NH_2$ terminal group after 3-APTES coating most likely enhanced the initial cell attachment, a phenomenon reported previously, of which human umbilical vein endothelial cells showed the best attachment efficiency on $-NH_2$ functionalized surface compared to − COOH, −OH and − CH_3 grafted surfaces.[34] However, the adverse effects of 3-APTES coating were seen after 3 days of culture.

Cell Morphology and Biointegration on Modified PMMA Surface. The cell morphology and expression of cell adhesion markers of human corneal stromal fibroblasts at day 3 after seeding on glass coverslip (control), untreated PMMA and modified PMMA surfaces are shown in Figure 8. Cell morphology observed in plasma group appeared similar to the control, which showed the typical slender morphology of fibroblast with prominent actin cytoskeleton spanning the length of cells.[35] In addition, prominent anchorage of cells to the modified surfaces was evident by the expression of focal adhesion proteins, paxillin and vinculin, at the cell periphery. In contrast, fewer cells stayed on untreated PMMA and 3-APTES coated PMMA, and they appeared round with reduced adherence to the surface. Cells on d-CaP and p-CaP, showed more prominent actin cytoskeleton. Most of them, however, appeared thinner and more spindle-shaped compared to cells on glass surface. Although CaP agglomerates generate huge

DOI: 10.1021/acsami.5b07621
ACS Appl. Mater. Interfaces 2015, 7, 21690−21702

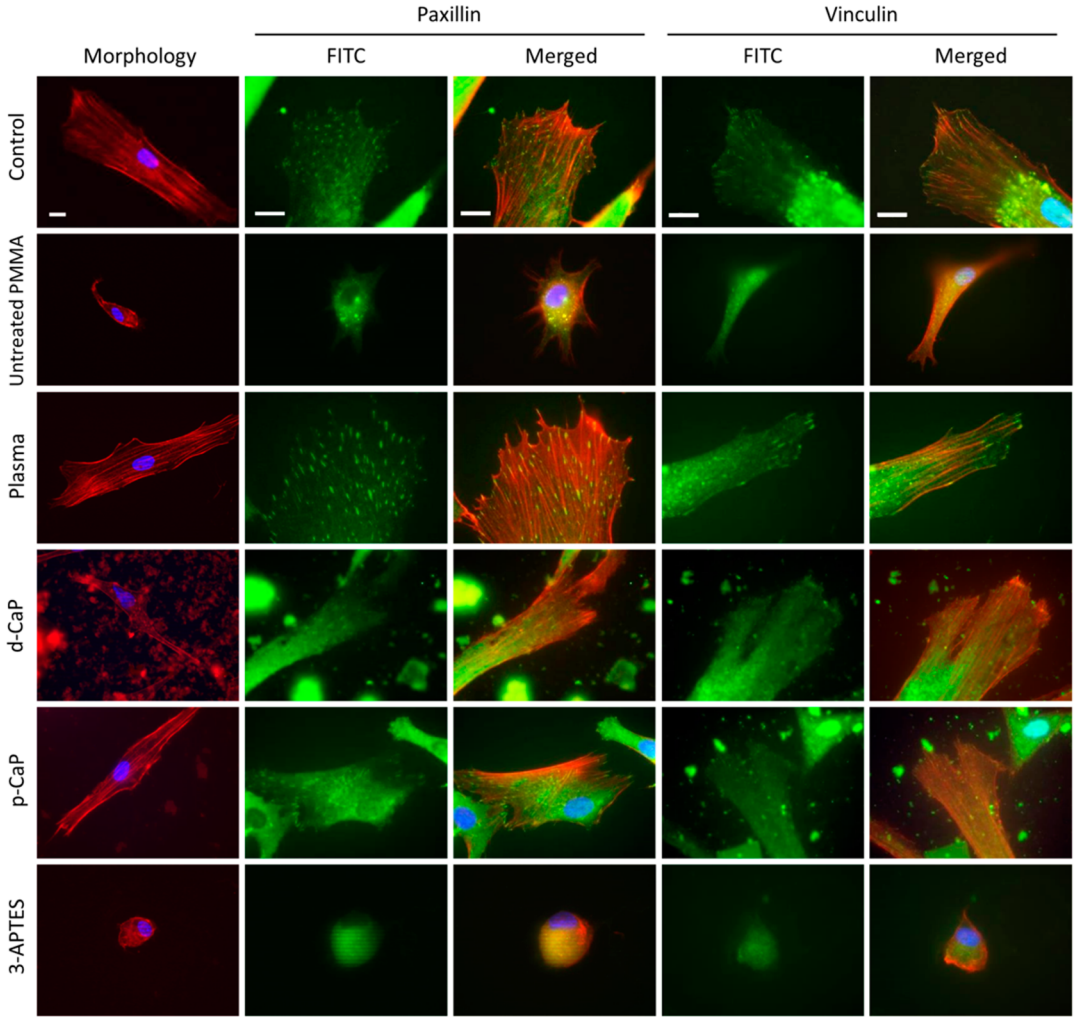

Figure 8. Cell morphology and attachment on modified PMMA surfaces on cell culture day 3. Cell morphology was assessed by staining of f-actin marker, phalloidin (red fluorescence). The ability of cells to attach on the modified PMMA surfaces was studied by expression of cell adhesion markers, paxillin and vinculin (green fluorescence). Nuclei (blue fluorescence) was stained with DAPI. Scale bars = 20 μm.

autofluorescent background, we still could detect the expression of paxillin and vinculin in the adherent cells.

This cell adherence phenomenon on different coated PMMA surfaces were confirmed by SEM. The fibroblasts seeded on glass coverslip showed extensive filopodia protrusions at the cell periphery, indicating prominent cell anchorage (Figure S5A). Similar observation was made for cells grown on plasma treated PMMA (Figure S5C). Cells seeded on either d-CaP (Figure S5D) or p-CaP (Figure S5E) appeared more spindle-shaped, but still featured prominent filopodia protrusions. In contrast, fibroblasts cultured on untreated PMMA (Figure S5B) and 3-APTES treated PMMA (Figure S5F) appeared round with rare filopodia protrusions.

It remains to be seen whether the biointegration of soft tissue, such as the cornea, to hard materials, such as PMMA can be enhanced by direct cell adhesion, material interaction with cell-secreted extracellular matrix and proteins, or both. However, studies on cells contributing to the adhesion and biointegration of hard tissue, such as bone, on hard materials appear to suggest this possibility.[36,37] The fact that corneal stromal cells survived and formed good adhesion on the CaP-coated PMMA surface suggests a potential benefit of the CaP coating in long-term conservation of the material biointegration, thus improving the clinical outcomes of the KPro device.

A limitation associated with the current study is that the hydrogels were acellular; however, the initial adhesion occurred with the acellular collagen. Similar to other implants, long-term survival of a KPro in the body is subject to many events including (but not limited to) cellular infiltration. In vivo, corneal stromal cells are normally in quiescent state, and their migration rate is slow.[38] Studies on the interactions between PMMA and collagen (with cells) can only follow in the wake of initial adhesion of the interfaces and are planned for later.

It should also be mentioned that the acellular hydrogel-modified PMMA constructs that we showed here were intended to model a synthetic core−skirt KPro, which would eliminate the use of human donor cornea as skirt material. Not only will the use of hydrogel reduce our reliance on donor corneas, but it can also reduce long-term complications normally associated with donor corneal transplantation due to immunologic reaction elicited by donor cells.[39] The collagen hydrogels are similar to those that have been implanted as an acellular artificial cornea in an ongoing human clinical trial, and have been shown to promote host cellular regeneration within months postimplantation.[40] Nevertheless, it is still important to maintain the stability of the interfacial adhesion before the stromal cells populate the scaffold, biointegrate, and subsequently provide further and more permanent stability to the

DOI: 10.1021/acsami.5b07621
ACS Appl. Mater. Interfaces 2015, 7, 21690−21702

KPro. The roles of stromal cells, which migrate into the artificial matrix, in the biointegration of soft material to CaP-coated PMMA warrant a separate and in-depth molecular level investigation.

CONCLUSIONS

We have shown that d-CaP not only enhanced the interfacial adhesion with collagen type I hydrogel, but also provided stability over a longer period of time compared to p-CaP. In addition, d-CaP provided a surface that was biocompatible, which allowed good biointegration with corneal stromal fibroblasts. Ultimately, the synthetic core−skirt KPro is aimed at reducing the heavy dependence on transplant-grade human donor corneas in the near future and reducing long-term complications associated with conventional KPro.

ASSOCIATED CONTENT

Supporting Information

The Supporting Information is available free of charge on the ACS Publications website at DOI: 10.1021/acsami.5b07621.

Additional experiments and supplementary table and figures regarding optimization of plasma treatment, biointegration of stromal fibroblasts on modified PMMA, and long-term performance of calcium phosphate coating on PMMA. (PDF)

AUTHOR INFORMATION

Corresponding Authors

*Phone: (65) 6790 4259. E-mail: assubbu@ntu.edu.sg.
*Fax: (65) 6322 7478. E-mail: jodmehta@gmail.com.

Notes

The authors declare no competing financial interest.

ACKNOWLEDGMENTS

This study was supported by Singapore National Medical Research Council funded Translational and Clinical Research (TCR) Flagship Programme (NMRC/TCR/008-SERI/2013).

REFERENCES

(1) Whitcher, J. P.; Srinivasan, M.; Upadhyay, M. P. Corneal Blindness: A Global Perspective. *Bull. World Health Organ.* **2001**, *79*, 214−221.
(2) Pascolini, D.; Mariotti, S. P. Global Estimates of Visual Impairment 2010. *Br. J. Ophthalmol.* **2012**, *96*, 614−618.
(3) Tan, D. T.; Dart, J. K.; Holland, E. J.; Kinoshita, S. Corneal Transplantation. *Lancet* **2012**, *379*, 1749−1761.
(4) Childress, J. F. Ethical Criteria for Procuring and Distributing Organs for Transplantation. *J. Health Polit. Policy Law* **1989**, *14*, 87−113.
(5) Muraine, M. C.; Collet, A.; Brasseur, G. Deep Lamellar Keratoplasty Combined with Cataract Surgery. *Arch. Ophthalmol.* **2002**, *120*, 812−815.
(6) Ilhan-Sarac, O.; Akpek, E. K. Current Concepts and Techniques in Keratoprosthesis. *Curr. Opin. Ophthalmol.* **2005**, *16*, 246−250.
(7) Gomaa, A.; Comyn, O.; Liu, C. Keratoprostheses in Clinical Practice − A Review. *Clin Exp Ophthalmol.* **2010**, *38*, 211−224.
(8) Nouri, M.; Terada, H.; Alfonso, E. C.; Foster, C. S.; Durand, M. L.; Dohlman, C. H. Endophthalmitis after Keratoprosthesis: Incidence, Bacterial Causes, and Risk Factors. *Arch. Ophthalmol.* **2001**, *119*, 484−489.
(9) Garcia, J. P., Jr; de la Cruz, J.; Rosen, R. B.; Buxton, D. F. Imaging Implanted Keratoprostheses with Anterior-Segment Optical Coherence Tomography and Ultrasound Biomicroscopy. *Cornea* **2008**, *27*, 180−188.
(10) Wang, L.; Jeong, K. J.; Chiang, H. H.; Zurakowski, D.; Behlau, I.; Chodosh, J.; Dohlman, C. H.; Langer, R.; Kohane, D. S. Hydroxyapatite for Keratoprosthesis Biointegration. *Invest. Ophthalmol. Visual Sci.* **2011**, *52*, 7392−7399.
(11) Martin, H. J.; Schulz, K. H.; Bumgardner, J. D.; Walters, K. B. XPS Study on the Use of 3-aminopropyltriethoxysilane to Bond Chitosan to a Titanium Surface. *Langmuir* **2007**, *23*, 6645−6651.
(12) Kim, K.; Park, S. W.; Yang, S. S. The Optimization of PDMS-PMMA Bonding Process Using Silane Primer. *BioChip J.* **2010**, *4*, 148−154.
(13) DiVito, M. D.; Rudisill, S. G.; Stein, A.; Patel, S. V.; McLaren, J. W.; Hubel, A. Silica Hybrid for Corneal Replacement: Optical, Biomechanical, and Ex Vivo Biocompatibility Studies. *Invest. Ophthalmol. Visual Sci.* **2012**, *53*, 8192−8199.
(14) Newsome, D. A.; Foidart, J. M.; Hassell, J. R.; Krachmer, J. H.; Rodrigues, M. M.; Katz, S. I. Detection of Specific Collagen Types in Normal and Keratoconus Corneas. *Invest. Ophthalmol. Vis. Sci.* **1981**, *20*, 738−750.
(15) Kokubo, T.; Kushitani, H.; Sakka, T.; Kitsugi, T.; Yamamuro, T. Solutions Able to Reproduce In Vivo Surface-Structure Changes in Bioactive Glass-Ceramic A-W. *J. Biomed. Mater. Res.* **1990**, *24*, 721−734.
(16) Liu, Y.; Gan, L.; Carlsson, D. J.; Fagerholm, P.; Lagali, N.; Watsky, M. A.; Munger, R.; Hodge, W. G.; Priest, D.; Griffith, M. A Simple, Cross-Linked Collagen Tissue Substitute for Corneal Implantation. *Invest. Ophthalmol. Visual Sci.* **2006**, *47*, 1869−1875.
(17) Salic, A.; Mitchison, T. J. A Chemical Method for Fast and Sensitive Detection of DNA Synthesis In Vivo. *Proc. Natl. Acad. Sci. U. S. A.* **2008**, *105*, 2415−2420.
(18) Fernandes da Silva, A. L.; Borba, A. M.; Simao, N. R.; Pedro, F. L.; Borges, A. H.; Miloro, M. Customized Polymethyl Methacrylate Implants for the Reconstruction of Craniofacial Osseous Defects. *Case Rep. Surg.* **2014**, *2014*, 358569.
(19) Srikumaran, D.; Munoz, B.; Aldave, A. J.; Aquavella, J. V.; Hannush, S. B.; Schultze, R.; Belin, M.; Akpek, E. K. Long-Term Outcomes of Boston Type 1 Keratoprosthesis Implantation: A Retrospective Multicentre Cohort. *Ophthalmology* **2014**, *121*, 2159−2164.
(20) Cortes, N. J.; Lloyd, J. M.; Koziol, L.; O'Hara, L. Successful Clinical Use of Daptomycin Impregnated Bone Cement in Two-Stage Revision Hip Surgery for Prosthetic Joint Infection. *Ann. Pharmacother.* **2013**, *47*, e2.
(21) Borges, A. M.; Benetoli, D.; Licinio, M. A.; Zoldan, V. C.; Santos-Silva, M. C.; Assreuy, J.; Pasa, A. A.; Debacher, N. A.; Soldi, V. Polymer Films with Surfaces Unmodified and Modified by Non-Thermal Plasma as New Substrates for Cell Adhesion. *Mater. Sci. Eng., C* **2013**, *33*, 1315−1324.
(22) Schaffner, P.; Meyer, J.; Dard, M.; Wenz, R.; Nies, B.; Verrier, S.; Kessler, H.; Kantlehner, M. Induced Tissue Integration of Bone Implants by Coating with Bone Selective RGD-Peptides In Vitro and In Vivo studies. *J. Mater. Sci.: Mater. Med.* **1999**, *10*, 837−839.
(23) Ryu, J.; Ku, S. H.; Lee, H.; Park, C. B. Mussel-Inspired Polydopamine Coating as a Universal Route to Hydroxyapatite Crystallization. *Adv. Funct. Mater.* **2010**, *20*, 2132−2139.
(24) Walsh, W. R.; Guzelsu, N. Compressive Properties of Cortical Bone − Mineral Organic Interfacial Bonding. *Biomaterials* **1994**, *15*, 137−145.
(25) Yang, C.; Cheng, K.; Weng, W.; Yang, C. Immobilization of RGD Peptide on HA Coating Through a Chemical Bonding Approach. *J. Mater. Sci.: Mater. Med.* **2009**, *20*, 2349−2352.
(26) Ozgen, O.; Aksoy, E. A.; Hasirci, V.; Hasirci, N. Surface Characterization and Radical Decay Studies of Oxygen Plasma-Treated PMMA Films. *Surf. Interface Anal.* **2013**, *45*, 844−853.
(27) Tang, L.; Lee, N. Y. A Facile Route for Irreversible Bonding of Plastic-PDMS Hybrid Microdevices at Room Temperature. *Lab Chip* **2010**, *10*, 1274−1280.
(28) Biqi, A.; Boanini, E.; Panzavolta, S.; Rovery, N.; Rubini, K. Bonelike Apatite Growth on Hydroxyapatite-Gelatin Sponges from Simulated Body Fluid. *J. Biomed. Mater. Res.* **2002**, *59*, 709−715.

DOI: 10.1021/acsami.5b07621
ACS Appl. Mater. Interfaces 2015, 7, 21690−21702

(29) Guckenberger, D. J.; Berthier, E.; Young, E. W.; Beebe, D. J. Induced Hydrophobic Recovery of Oxygen Plasma-Treated Surfaces. *Lab Chip* **2012**, *12*, 2317−2321.
(30) Fritz, J. L.; Owen, M. J. Hydrophobic Recovery of Plasma-Treated Polydimethylsiloxane. *J. Adhes.* **1995**, *54*, 33−45.
(31) Howarter, J. A.; Youngblood, J. P. Surface Modification of Polymers with 3- aminopropyltriethoxysilane as a General Pretreatment for Controlled Wettability. *Macromolecules* **2007**, *40*, 1128−1132.
(32) Olde Damink, L. H.; Dijkstra, P. J.; van Luyn, M. J.; van Wachem, P. B.; Nieuwenhuis, P.; Feijen, J. Cross-Linking of Dermal Sheep Collagen Using a Water-Soluble Carbodiimide. *Biomaterials* **1996**, *17*, 765−773.
(33) Dupraz, A. M.; de Wijn, J. R.; v d Meer, S. A.; de Groot, K. Characterization of Silane Treated Hydroxyapatite Powders for Use as Filler in Biodegradable Composites. *J. Biomed. Mater. Res.* **1996**, *30*, 231−238.
(34) Arima, Y.; Iwata, H. Effects of Surface Functional Groups on Protein Adsorption and Subsequent Cell Adhesion Using Self-Assembled Monolayers. *J. Mater. Chem.* **2007**, *17*, 4079−4087.
(35) Wilson, S. L.; El Haj, A. J.; Yang, Y. Control of Scar Tissue Formation in the Cornea: Strategies in Clinical and Corneal Tissue Engineering. *J. Funct. Biomater.* **2012**, *3*, 642−687.
(36) Riedel, N. A.; Williams, J. D.; Popat, K. C. Ion Beam Etching Titanium for Enhanced Osteoblast Response. *J. Mater. Sci.* **2011**, *46*, 6087−6095.
(37) Liu, H.; Slamovich, E. B.; Webster, T. J. Increased Osteoblast Functions on Nanophase Titania Dispersed in Poly-lactic-co-glycolic Acid Composites. *Nanotechnology* **2005**, *16*, S601−S608.
(38) West-Mays, J. A.; Dwivedi, D. J. The Keratocyte: Corneal Stromal Cell with Variable Repair Phenotypes. *Int. J. Biochem. Cell Biol.* **2006**, *38*, 1625−1631.
(39) Guilbert, E.; Bullet, J.; Sandali, O.; Basli, E.; Laroche, L.; Borderie, V. M. Long-Term Rejection Incidence and Reversibility after Penetrating and Lamellar Keratoplasty. *Am. J. Ophthalmol.* **2013**, *155*, 560−569.
(40) Fagerholm, P.; Lagali, N. S.; Ong, J. A.; Merrett, K.; Jackson, W. B.; Polarek, J. W.; Suuronen, E. J.; Liu, Y.; Brunette, I.; Griffith, M. Stable Corneal Regeneration Four Years after Implantation of a Cell-Free Recombinant Human Collagen Scaffold. *Biomaterials* **2014**, *35*, 2420−2427.

DOI: 10.1021/acsami.5b07621
ACS Appl. Mater. Interfaces 2015, 7, 21690−21702